Translocation of Single-Stranded DNA Through Single-Walled Carbon Nanotubes

Haitao Liu *et al.*

Science **327**, 64 (2010);
DOI: 10.1126/science.1181799

electric field imposed on minority electrons injected into the p-type layer of the graded AlGaN. The compositional grading in the p-type AlGaN layer causes the increase in the band gap ΔE_g to appear entirely in the conduction band, which acts as a natural electron-blocking layer. This feature is shown in the energy-band diagram in Fig. 4D. Electron-blocking layers have been shown to improve the efficiency of emission by preventing the spillover of higher mobility electrons from the optically active regions of nitride LEDs (*20*). Conventional electron-blocking layers implemented in nitride LEDs and lasers consist of a thin AlGaN layer placed on the p-doped side [schematic band diagram shown in Fig. 4C]. In addition to blocking electron overflow through a conduction band barrier ΔE_C, such layers also prevent efficient hole injection because of the unavoidable valence-band offset ΔE_V (*21*). Polarization-doped graded layers provide a solution to this design bottleneck. In addition to improving the p-type conductivity, the polarization-induced graded p-type AlGaN layer facilitates electron blocking without adding barriers to hole injection and offers an added degree of freedom in graded–refractive-index design, all of which are useful for UV laser applications. The polarization-doped layer is also of a larger band gap than the active region of the p-n junction and serves as a natural optically transparent layer with minimal absorption losses.

This method of polarization doping should prove particularly useful for deep-UV optoelectronic applications where both p- and n-type doping of high Al composition AlGaN is a major challenge. The technique presented here could be applied to produce highly conductive p-type regions in wide–band-gap nitrides composed of high–Al composition AlGaN and in the more general AlInGaN material system with proper choice of the crystal direction of growth and management of strain within allowable limits. The doping scheme can be used to obtain desired hole or electron concentrations in spite of poor ionization efficiencies of deep-level dopants in any semiconductor crystals that possess sufficiently strong spontaneous and piezoelectric polarization (for example, in the ZnO material family).

References and Notes

1. Y. Taniyasu, M. Kasu, T. Makimoto, *Nature* **441**, 325 (2006).
2. A. Khan, K. Balakrishnan, T. Katona, *Nat. Photonics* **2**, 77 (2008).
3. D. A. Steigerwald *et al.*, *IEEE J. Sel. Top. Quantum Electron.* **8**, 310 (2002).
4. O. Brandt, K. H. Ploog, *Nat. Mater.* **5**, 769 (2006).
5. P. Kozodoy *et al.*, *J. Appl. Phys.* **87**, 1832 (2000).
6. W. Götz, N. M. Johnson, J. Walker, D. P. Bour, R. A. Street, *Appl. Phys. Lett.* **68**, 667 (1996).
7. C. J. Eiting, P. A. Grudowski, R. D. Dupuis, *Electron. Lett.* **33**, 1987 (1997).
8. F. Bernardini, V. Fiorentini, D. Vanderbilt, *Phys. Rev. B* **56**, R10024 (1997).
9. C. Wood, D. Jena, *Polarization Effects in Semiconductors: From Ab-Initio Theory to Device Applications* (Springer, New York, 2007).
10. Y. Cao, D. Jena, *Appl. Phys. Lett.* **90**, 182112 (2007).
11. Y.-F. Wu *et al.*, *IEEE Electron Device Lett.* **25**, 117 (2004).
12. I. D. Goepfert, E. F. Schubert, A. Osinsky, P. E. Norris, *Electron. Lett.* **35**, 1109 (1999).
13. P. Kozodoy, M. Hansen, S. P. DenBaars, U. K. Mishra, *Appl. Phys. Lett.* **74**, 3681 (1999).
14. J. Simon, A. K. Wang, H. Xing, S. Rajan, D. Jena, *Appl. Phys. Lett.* **88**, 042109 (2006).
15. D. Jena *et al.*, *Phys. Rev. B* **67**, 153306 (2003).
16. S. Rajan, H. Xing, S. DenBaars, U. K. Mishra, D. Jena, *Appl. Phys. Lett.* **84**, 1591 (2004).
17. S. Rajan *et al.*, *Appl. Phys. Lett.* **102**, 044501 (2007).
18. Details of the growth and fabrication procedure are described in the supporting online material.
19. F. Calle *et al.*, *MRS Internet J. Nitride Semicond. Res.* **3**, article 24 (1998).
20. R.-C. Tu *et al.*, *IEEE Photon. Technol. Lett.* **15**, 1342 (2003).
21. S.-H. Han *et al.*, *Appl. Phys. Lett.* **94**, 231123 (2009).

22. We thank the U.S. Office of Naval Research and the NSF (award no. 0907583) for financial support and C. Wood for discussions. N-face semi-insulating substrates were obtained from D. Hanser, Kyma Technologies, Raleigh, North Carolina.

Supporting Online Material

www.sciencemag.org/cgi/content/full/327/5961/60/DC1
Materials and Methods
Figs. S1 to S3
References

12 October 2009; accepted 30 October 2009
10.1126/science.1183226

Translocation of Single-Stranded DNA Through Single-Walled Carbon Nanotubes

Haitao Liu,[1]* Jin He,[2]* Jinyao Tang,[1] Hao Liu,[2,3] Pei Pang,[2,4] Di Cao,[2,4] Predrag Krstic,[5] Sony Joseph,[5] Stuart Lindsay,[2,3,4]† Colin Nuckolls[1]†

We report the fabrication of devices in which one single-walled carbon nanotube spans a barrier between two fluid reservoirs, enabling direct electrical measurement of ion transport through the tube. A fraction of the tubes pass anomalously high ionic currents. Electrophoretic transport of small single-stranded DNA oligomers through these tubes is marked by large transient increases in ion current and was confirmed by polymerase chain reaction analysis. Each current pulse contains about 10^7 charges, an enormous amplification of the translocated charge. Carbon nanotubes simplify the construction of nanopores, permit new types of electrical measurements, and may open avenues for control of DNA translocation.

We report the use of single-walled carbon nanotubes (SWCNTs) as nanopores for analyzing molecular transport properties. Nanopores are orifices of molecular diameter that connect two fluid reservoirs. At this length scale, the passage of even a single molecule generates a detectable change in the flow of ionic current through the pore (*1*, *2*). They can be used as single-molecule Coulter counters and form the basis of proposed new approaches to DNA sequencing (*3*). The first nanopore devices were based on pore proteins (*4*–*7*), but more recently pores have been fabricated by drilling (and sometimes partially refilling) solid-state materials (*8*–*12*). Nanochannels have been formed by etching silicon nanowires (*13*), and channels with one nanoscale dimension have been etched into glass (*14*) or quartz (*15*).

Carbon nanotubes are obvious candidates for the fabrication of nanopore structures. Pressure-driven gas, water, and ion transport has been recorded through membranes composed of many multiwalled carbon nanotubes (*16*) or double-walled carbon nanotubes (*17*). These experiments showed that the water flow rate is greatly enhanced inside the tube, an effect confirmed by molecular dynamics simulations (*18*). DNA has been passed through a 100-nm diameter carbon nanotube (*19*) and 50-nm-wide hydrophilic channels (*13*). It seems counterintuitive that hydrophilic DNA would enter the hydrophobic interior of a SWCNT, but simulations show that both RNA (*20*) and DNA (*21*) will translocate through 1.5- to 2-nm diameter tubes. The simulations were carried out using very large electric fields (tenths of a volt per nm) to generate observable motion on the simulation time scale. This result leaves open the possibility that some measurable translocation might occur at the much smaller fields that could be implemented in the laboratory. Here, we report direct measurement of this translocation.

We have made a device in which one SWCNT spans a barrier between two fluid reservoirs [see Fig. 1 and Supporting Online Material (*22*)]. Relative to CNT membranes (*16*, *17*), this arrangement makes it possible to detect signals from the translocation of a single molecule and to correlate

[1]Department of Chemistry, Columbia University, New York, NY 10027, USA. [2]Biodesign Institute, Tempe, AZ 85287, USA. [3]Department of Chemistry and Biochemistry, Tempe, AZ 85287, USA. [4]Department of Physics, Arizona State University, Tempe, AZ 85287, USA. [5]Physics Division, Oak Ridge National Laboratory, Oak Ridge, TN 37831, USA.

*These authors contributed equally to this work.
†To whom correspondence should be addressed. E-mail: Stuart.Lindsay@asu.edu (S.L.); cn37@columbia.edu (C.N.)

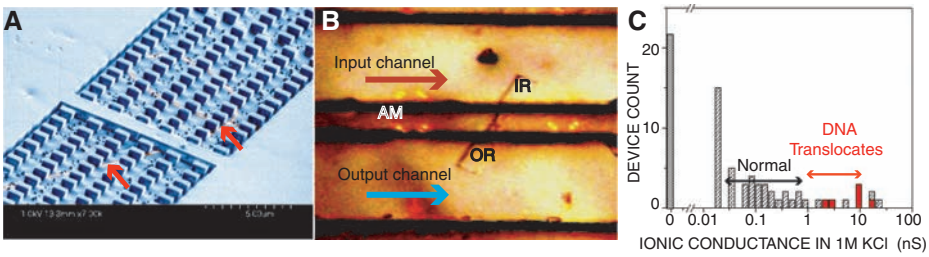

Fig. 1. (**A**) A single nanopore device was fabricated by growing SWCNTs at low densities on an oxidized Si wafer. We used cobalt catalyst particles with ethanol vapor as the carbon source in conditions most likely to produce high-quality SWCNTs with an outside diameter of 1 to 2 nm (*30*). A 700-nm layer of PMMA resist is spun on and reservoirs opened over selected tubes with electron-beam lithography. The exposed regions of SWCNTs were removed by O_2 plasma etch. The SEM image of the device shows a 2-μm barrier before removal of the exposed SWCNT (arrows). Pillars in the reservoir support the PDMS cover. (**B**) Optical micrograph taken through a PDMS cover. The reservoirs (IR, input; OR, output) span the barrier between PDMS channels at an angle of about 60°. AM marks the location of one set of alignment markers. (**C**) Current flows through the single SWCNTs and not through a leakage path. With the SWCNT bridging the gap and opened, most tubes pass currents in the expected range (Normal), but 20% pass unexpectedly large currents. Some of these (marked in red) also passed DNA oligomers. These data are limited to the subset of devices exposed to short plasma etches for which control experiments show no leakage (*22*).

Table 1. Relation of ionic conductance with electrical properties (V_T is the threshold voltage for semiconducting tubes). These measurements do not discriminate between metallic SWCNTs and bundles containing a metallic tube, but most of the tubes are single-walled (*30*). Raman scattering was used to determine diameters marked * and confirm electronic properties marked †. The tube marked ‡ translocated DNA.

FET device ID	Ionic current	Diameter (nm)	Electrical property
HL_4_1_41 AP3	10.7 ± 0.05 nA/0.4 V	2.0	Metallic
HL_4_1_10 AB6	3.4 ± 0.04 nA/0.5 V	1.7 (1.5*)	Metallic†
HL_4_1_39 P6	2.5 ± 0.07 nA/0.4 V‡	4.2	Metallic
HL_4_1_41 AZ3	1.91 ± 0.05 nA/0.4 V	–	Metallic
HL_4_1_41 N2	0.98 ± 0.04 nA/0.4 V (V_T ~ 10 V)	0.9	Semiconducting
HL_4_1_37 AB20	0.46 ± 0.03 nA/0.5 V (V_T ~ 10 V)	1.3*	Semiconducting†
HL_4_1_41 AS3	0.07 ± 0.02 nA/0.4 V (V_T ~ 25 V)	1.8	Semiconducting
HL_4_1_37 Z22	0.10 ± 0.03 nA/0.5 V (V_T ~ 10 V)	1.1*	Semiconducting†
HL_4_1_41 M8	<10 pA/0.4 V(V_T ~ 25V)	3.4	Semiconducting

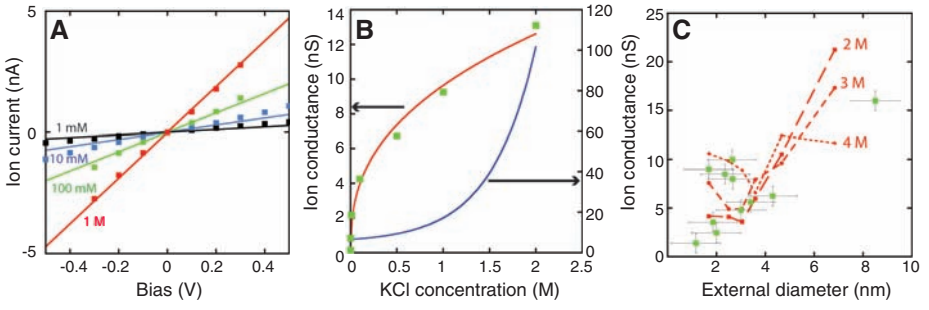

Fig. 2. Ion transport in the subset of SWCNTS with high ionic conductance. (**A**) Current versus voltage applied to Ag/AgCl reference electrodes for a 2-μm long, 1.7-nm diameter SWCNT for various concentrations of KCl electrolyte as marked. The solid lines are simulated as described in the text. (**B**) Ionic conductance as a function of salt concentration. The red line is a fit to the c^m dependence suggested by molecular dynamics simulations. We found $0.33 < m < 0.4$ in three different tubes. The blue line shows the salt dependence of conductance measured in a planar nanopore (*27*). (**C**) In this subset of tubes, current at 1 M KCl is better related to diameter (green squares). The red dashed lines show simulations for excess charge densities of 2, 3, and 4 M.

transport with the properties of individual SWCNTs. We grew well-separated SWCNTs on the surface of oxidized silicon wafers and formed fluid reservoirs along the path of chosen tubes with electron-beam lithography. A scanning electron microscopy (SEM) image of a device at this stage is shown in Fig. 1A, where the SWCNT is just visible on each side of the barrier. An oxygen plasma was used to remove the exposed parts of the SWCNT, leaving the SWCNT under the barrier intact (fig. S4I) (*22*, *23*). The fluidic pathway was completed by placing a poly(dimethylsiloxane) (PDMS) cover on top of the chip (Fig. 1B).

Each chip also contained control devices lacking the bridging SWCNT (*22*) to check the integrity of the barrier, including devices with unopened SWCNTs. We used a mild plasma treatment such that 100% of the devices lacking CNTs did not leak (fig. S5), although this approach resulted in a large fraction of tubes that were not opened (20%), as determined by SEM imaging (fig. S4F). The fluid reservoirs were filled with 1 M KCl, and Ag/AgCl electrodes (BASI MF-2078) were used to measure the conductance across the reservoirs connected by the SWCNT. The devices passed current if, and only if, they were spanned by a SWCNT that was opened (Fig. 1C), so the interface between the tube and the poly(methyl methacrylate) (PMMA) does not appear to provide a leakage path. This conclusion was verified by chemically tethering poly(ethylene glycol) molecules to one or both ends of the CNTs. The current was reduced in one direction of bias when the tube was modified at one end, and in both directions of bias when the tube was modified at both ends (fig. S6).

The ionic conductance of a tube of electrolyte should be given by $G = 6.02 \times 10^{26}\,(\mu_K + \mu_{Cl})c_{KCl}e\pi D^2/4L$, where $\mu_K = 7.62 \times 10^{-8}$ m^2/V s, $\mu_{Cl} = 7.91 \times 10^{-8}$ m^2/V s, c_{KCl} is the KCl concentration in mole/l, e the electronic charge, D the tube diameter, and L the tube length. Table 1 shows that there is no correlation between the tube diameter and ionic conductance. The ionic conductance spans nearly four orders of magnitude (Fig. 1C), with only the lowest conductances (the range marked "normal" in Fig. 1C) being consistent with the classical formula for c_{KCl} = 1 M, 1 nm < D < 5 nm (fig. S7) and L = 2 μm. We also measured the electronic properties of some of the tubes (Table 1) using both their response as field-effect transistors and Raman scattering (figs. S8 to S10). The SWCNTs with the highest ionic conductance are all metallic.

We considered whether the excess current could be accounted for by electrochemical currents stemming from reduction and oxidation reactions at the end of metallic tubes. A conducting tube suspended in a potential gradient in an electrolyte acts as a bipolar electrode (*24*), but enormous fields are required to drive electrochemical processes at the ends of a bipolar carbon nanotube electrode (*25*). Measurements with

an electrode contacting the SWCNT directly revealed that electrochemical currents were negligible for the potentials used here (fig. S11).

To look for clues to a mechanism for the large ionic currents, we used molecular dynamics simulations coupled with solutions of the Poisson-Nernst-Planck equation for transport in the SWCNT and the outside reservoirs (*22*). The flow rate of water is greatly enhanced inside SWCNTs (*17*), but the molecular dynamics simulations showed that the electrophoretic mobility of ions is similar to that in the bulk electrolyte. However, the selective filtering of anions or cations owing to charged end groups (*26*) can result in a net excess concentration, n, of one charge inside the tube. This charge will, in turn, drive an electroosmotic current. Molecular dynamics simulations further showed that both water and ions flow with an electroosmotic velocity, v, given by $v \propto n^{0.74}$ for a (10,10) SWCNT. Both anions and cations are driven in the same direction by an extremely large electroosmotic flow, but only the charge imbalance inside the tube results in a net ionic current proportional to nv, that is, $\propto n^{1.74}$. The mechanism of charge accumulation is complex and involves both charged end groups and the electronic properties of the SWCNT, and we have not yet developed a quantitative model for it (see fig. S12 for further evidence of the role of charged end groups). However, current-voltage curves obtained at different salt concentrations in the reservoirs, c, can be fitted if $n = 3.31\ c^{0.22}$ M (Fig. 2A). This result is equivalent to an ionic conductance that varies as $c^{0.39}$, shown by the red curve passing through the measured data in Fig. 2B. This dependence on concentration is quite different from the linear dependence expected for a tube of electrolyte or the saturation at low salt observed for a planar nanopore carrying a surface charge (*27*).

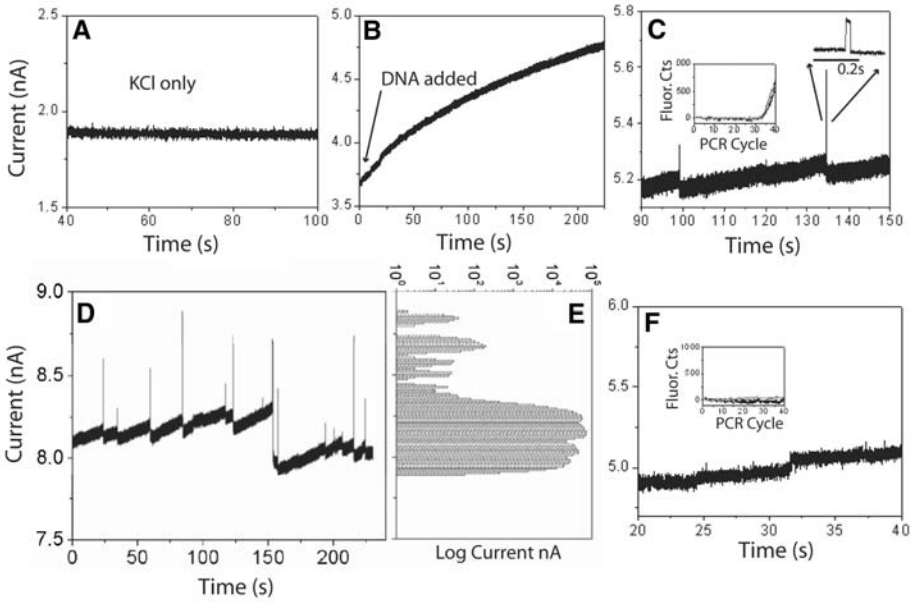

Fig. 3. Ion current signals of DNA translocation. (**A**) Current (2 M KCl, 1 mM PBS, pH 7) before DNA addition. (**B**) After DNA addition, current slowly increases. (**C**) 5 min after addition of 0.1-nM 60-nt DNA, large positive current spikes appear. These spikes are followed by a drop in baseline over a period of a second or so and then by a gradual rise leading to the next spike. (**D**) Representative data from another tube (also 60-nt DNA), with the distribution of currents shown in (**E**). The DNA causes large changes in baseline in addition to the spikes. (**F**) Data from a tube that showed both a current increase on DNA addition and baseline fluctuations but no spikes. No translocation was detected by PCR. The insets in (C) and (F) show the fluorescence signal from double-stranded DNA dye labels as a function of the PCR cycle number for samples collected from these particular runs.

Table 2. Results of QPCR tests for translocation in tubes with conductance >2 nS that gave uncontaminated control signals (data from four other devices that showed contamination in the control sample were rejected). Errors in spike count reflect the consequences of different cut-off criteria for selecting spikes. Errors in the molecule count were dominated by uncertainties in the filter recovery efficiency, except for the data marked *, which were calibrated with a second oligomer.

Tube	Tube conductance nS (1 M KCl)	DNA sample (nt)	Number of spikes	Number of molecules	Molecules per spike
AD1	9.7	60	350 ± 50	8000 ± 2000	23 ± 10
AD2	9.5	60	30 ± 10	400 ± 200	13 (+17, −13)
AA New1	19.6	120	64 ± 10	8500 ± 3100	88 (+126, −88)
AA New2	2.7	120	1500 ± 200	24,400 ± 5700	16 ± 7
HL-4-1-36	9.6	60	36 ± 4	1224 ± 774*	34 ± 21*
A136	1.6	60	46 ± 5	1900 ± 200*	41 ± 10*
HL-4-1-41	4.8	60	0	0	–
HL-4-1-40 O8	2.7	60	0	0	–

In contrast to the full set of devices, the subset with anomalously high conductance does show some relation between conductance and tube diameter (Fig. 2C, green squares). The red dashed lines show simulated values of ionic conductance as a function of diameter for n = 2, 3, and 4 M. The measured data can be accounted for by assuming that variability in the charge of end groups leads to some variability in n.

Although it might be instructive to study the translocation of simpler polyelectrolytes as a prelude to the study of DNA, methods such as dye-labeling are much less sensitive than polymerase chain reaction (PCR) for detecting and counting small numbers of molecules.

To test for DNA translocation of SWCNTs, we used 60-nt and 120-nt DNA oligomers with sequences that were predicted to be relatively free of secondary structure, with forward and reverse primers chosen to have high melting temperatures to minimize primer dimers and false priming (*22*). Devices were characterized by measuring current flow with 1 or 2 M KCl alone, and then a DNA solution [1 or 2 M KCl, 1 mM phosphate-buffered saline (PBS), pH 7] was flowed into the input reservoir side. A control sample was collected from the output reservoir to check for DNA contamination, and a positive bias was then applied to the output side of the device. In the subset of high current tubes, we first observed a slow increase in the background current (Fig. 3, A and B; data are for 0.1 nM DNA). After a time, which varied from a few to tens of minutes, depending on the DNA concentration in the input reservoir, large transient increases in current were observed. These "spikes" were accompanied by large fluctuations in the background current (Fig. 3C). The spikes disappeared when the polarity of the bias across the tube was reversed and reappeared when the original bias (positive on the output side) was restored. Quantitative PCR (QPCR) (*22*) showed that DNA was translocated in devices manifesting these large spikes. Translocation occurred only in tubes with conductances (before DNA addition) of >2 nS (Fig. 1C). Some devices that showed instabilities in the background but no large current spikes (Fig. 3F) gave negative PCR results. We also tested for transloca-

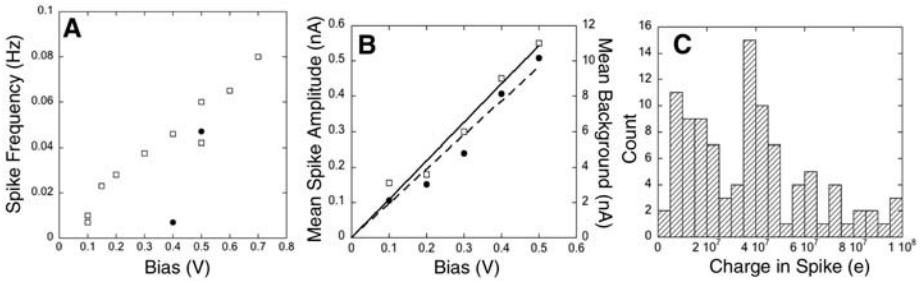

Fig. 4. Characteristics of the translocation signals for 60-nt DNA. (**A**) Spike rate increases with bias after a threshold that depends on the particular CNT; the two devices here show spike signals above 0.1 (squares) and 0.4 V (circles). (**B**) Spike amplitude (squares) increases linearly with bias and is about 5% of the background current (circles). (**C**) Distribution of the charge in each spike for the SWCNT in units of the electronic charge, *e*.

tion in "failed" control devices (i.e., lacking the CNT and deliberately overetched) that displayed leakage current. A few with very large leakage current showed evidence of DNA in the output well, but none displayed spikes, regardless of the magnitude of the leakage current. Thus, the spikes signal translocation of DNA through the SWCNTs.

QPCR also provides a measure of the number of molecules collected. We collected small samples of fluid from the output reservoir by flushing the system through with excess buffer and concentrated the solution using a Microcon YM-10 centrifugal filter so that we could redilute with PCR buffer. The filter losses were found to be highly variable, more so at low DNA concentrations, and account for much of the stated uncertainty in our results. We calibrated the PCR reaction with known amounts of DNA and, for two data points, calibrated filter losses by adding a known amount of a second sequence (with orthogonal primers) and carrying out a PCR analysis of both the target and calibration samples. The final molecule count was corrected for filter losses and dilution during the sample collection. The various errors in these steps tend to underestimate the amount of DNA that translocated, so the final results are probably lower limits. PCR was limited to the first use of a device, and we rejected samples from chips that showed contamination in the control samples collected.

We were able to carry out PCR on samples collected from 12 devices that had a conductance >2 nS. Of these, four had DNA contamination in control samples, leaving the eight devices listed in Table 2. Two of these showed no spikes and yielded no PCR signal. The remaining six all appeared to pass more than one molecule per spike. In particular, tubes HL-4-1-36 and A136, for which the filter recovery was directly measured with a control sample, passed at least 30 to 40 molecules for each spike. It is possible that the tube fills entirely with DNA, the spike signaling the cooperative emptying (or possibly filling) of the tube. The uncertainties in the PCR measurement are too large to reveal any significant difference between the number of molecules per spike for the 60-nt sample (23, 13, 34, and 41) and the 120-nt sample (88 and 16), although the spike frequency was much lower in the two 120-nt runs, and the spike duration significantly longer (figs. S13 and S14).

Figure 4A shows data for the spiking rate as a function of bias for two different tubes passing 60-nt DNA. The spike rate increased with applied bias, and the two tubes showed different threshold biases for the onset of spikes (and hence translocation). For the 60-nt DNA, the spike amplitudes are about 5% of the baseline current (Fig. 4B), and their duration is between 3 and 100 ms, independent of applied bias, as long as it is above the threshold for translocation. The product of the spike duration and amplitude yields the charge contained in each spike (Fig. 4C). This is remarkably large, at about 1 pC or 10^7 electrons in each spike. Fan *et al.* explained positive charge spikes observed in nanochannels as a consequence of additional mobile ions brought into the channel by DNA molecules (*13*). Filling the tubes (2 μm long) with 100 (20 nm long) 60-nt DNA oligomers, each carrying 60 excess electronic charges would account for only 1 part in 10,000 of the observed charge in each spike. The spikes must originate with large changes in the polarization outside the tubes, much as observed in junctions between micro- and nanochannels (*28*). The charge accumulation caused by the asymmetrical current in the SWCNT might be the source of this polarization, but further modeling is required to shed light on this unusual signal.

The excess ionic conductance appears to be a characteristic of metallic tubes, and we have proposed a mechanism based on electroosmotic flow resulting from trapped charge. Tubes with high ionic conductance will transport DNA molecules, giving a distinctive and unexpectedly large electrical signal of translocation. This kind of nanopore combines a long channel (in which translocation speed might be slowed) with an "integrated" electrode that might prove useful in new schemes for sequencing DNA by tunneling (*3*). The ability to select metallic SWCNTs of a desired diameter (*29*) may open the way for production of devices with particular pore sizes.

References and Notes

1. M. Rhee, M. A. Burns, *Trends Biotechnol.* **25**, 174 (2007).
2. C. Dekker, *Nat. Nanotechnol.* **2**, 209 (2007).
3. D. Branton *et al.*, *Nat. Biotechnol.* **26**, 1146 (2008).
4. J. J. Kasianowicz, E. Brandin, D. Branton, D. W. Deamer, *Proc. Natl. Acad. Sci. U.S.A.* **93**, 13770 (1996).
5. M. Akeson, D. Branton, J. J. Kasianowicz, E. Brandin, D. W. Deamer, *Biophys. J.* **77**, 3227 (1999).
6. J. Kasianowicz, S. Henrickson, H. Weetall, B. Robertson, *Anal. Chem.* **73**, 2268 (2001).
7. A. Meller, D. Branton, *Electrophoresis* **23**, 2583 (2002).
8. J. Li *et al.*, *Nature* **412**, 166 (2001).
9. A. Storm, J. Chen, X. Ling, H. Zandbergen, C. Dekker, *Nat. Mater.* **2**, 537 (2003).
10. H. Chang *et al.*, *Appl. Phys. Lett.* **88**, 103109 (2006).
11. M. J. Kim, M. Wanunu, D. C. Bell, A. Meller, *Adv. Mater.* **18**, 3149 (2006).
12. P. Chen *et al.*, *Nano Lett.* **4**, 1333 (2004).
13. R. Fan *et al.*, *Nano Lett.* **5**, 1633 (2005).
14. D. Stein, M. Kruithof, C. Dekker, *Phys. Rev. Lett.* **93**, 035901 (2004).
15. X. Liang, S. Y. Chou, *Nano Lett.* **8**, 1472 (2008).
16. B. J. Hinds *et al.*, *Science* **303**, 62 (2004).
17. J. K. Holt *et al.*, *Science* **312**, 1034 (2006).
18. S. Joseph, N. R. Aluru, *Nano Lett.* **8**, 452 (2008).
19. T. Ito, L. Sun, R. M. Crooks, *Chem. Commun.* **2003**, 1482 (2003).
20. I.-C. Yeh, G. Hummer, *Proc. Natl. Acad. Sci. U.S.A.* **101**, 12177 (2004).
21. Y. Xie, Y. Kong, A. K. Soh, H. Gao, *J. Chem. Phys.* **127**, 225101 (2007).
22. Materials and methods are available as supporting material on *Science* Online.
23. We also made some devices using multiwalled tubes but found that these were much more difficult to open (fig. S3) (*22*).
24. K.-F. Chow, F. Mavre, R. M. Crooks, *J. Am. Chem. Soc.* **130**, 7544 (2008).
25. C. Warakulwit *et al.*, *Nano Lett.* **8**, 500 (2008).
26. S. Joseph, R. J. Mashl, E. Jakkobsson, N. R. Aluru, *Nano Lett.* **3**, 1399 (2003).
27. R. M. M. Smeets *et al.*, *Nano Lett.* **6**, 89 (2006).
28. X. Jin, S. Joseph, E. Gatimu, P. Bohn, N. R. Aluru, *Langmuir* **23**, 13209 (2007).
29. X. Tu, S. Manohar, A. Jagota, M. Zheng, *Nature* **460**, 250 (2009).
30. X. Guo *et al.*, *Science* **311**, 356 (2006).

31. We acknowledge valuable discussions with G. Zhang, O. Sankey, D. Crooks, C. Yamashiro, and M. Muthukumar. X. Cui provided us with samples of larger-diameter SWCNTs, and T. Liu assisted us with atomic force microscopy measurements. This work was supported by grants from the DNA sequencing technology program of the National Human Genome Research Institute, Arizona Technology Enterprises, and the Biodesign Institute (S.L.), an NSF NIRT Award, Nanoscale Science and Engineering Initiative of the NSF, and NYSTAR (C.N.), the OFES, U.S. DOE, and NSF through the National Institute for Computational Sciences of the University of Tennessee (P.K.). A patent has been filed jointly by Arizona State University and Columbia University naming J. He, S. Lindsay, and C. Nuckolls as inventors in the area of DNA sequencing.

Supporting Online Material

www.sciencemag.org/cgi/content/full/327/5961/64/DC1
Materials and Methods
Figs. S1 to S14
Tables S1 to S3
References

10 September 2009; accepted 28 October 2009
10.1126/science.1181799